Title
ELASTIC SCATTERING OF 31-MeV He3 IONS FRCM SEVERAL ELEMENTS

Authors
Igo, George
Markowitz, Samuel S.
Vidal, Jose G.

Publication Date
1961-12-31

UCRL-9996

University of California

Ernest O. Lawrence Radiation Laboratory

Berkeley, California

DISCLAIMER

UCRL-9996

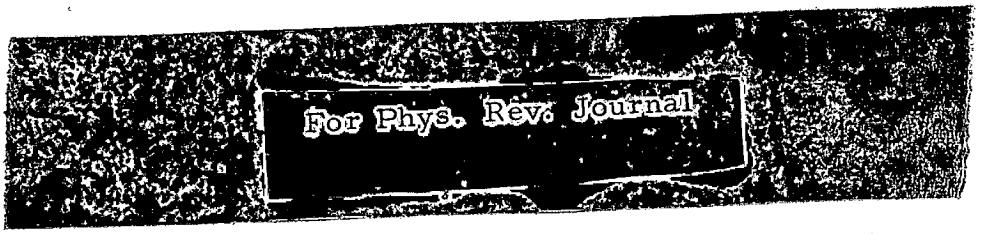

UNIVERSITY OF CALIFORNIA

Lawrence Radiation Laboratory
Berkeley, California

Contract No. W-7405-eng-48

ELASTIC SCATTERING OF 31-Mev He^3 IONS FROM SEVERAL ELEMENTS

George Igo, Samuel S. Markowitz, and Jose G. Vidal

December 31, 1961

ELASTIC SCATTERING OF 31-Mev He^3 IONS FROM SEVERAL ELEMENTS

Contents

ELASTIC SCATTERING OF 31-Mev He^3 IONS FROM SEVERAL ELEMENTS

George Igo and Jose G. Vidal

Lawrence Radiation Laboratory
University of California
Berkeley, California

and

Samuel S. Markowitz

Chemistry Department and Lawrence Radiation Laboratory,
University of California, Berkeley, California

December 31, 1961

ABSTRACT

The absolute differential cross sections for elastic scattering of 31-Mev He^3 ions on Be, Al, Cu, $Sn^{(nat)}$, Sn^{120}, and Bi have been measured in the angular range of approximately 10 to 120 deg in the center-of-mass system. Thin self-supporting foil targets were chosen to span the parameter $A^{1/3}$, where A is the target mass number. The first excited states of the isotopes of the above elements had sufficient energy separation from the ground state to enable elastic scattering to be resolved from inelastic scattering. The detection system, consisting of CsI(Tℓ) scintillation crystals, was capable of 3% pulse-height resolution and 1 degree angular resolution. Characteristically, the light-element angular distributions show strong diffraction effects. The differential cross section divided by the Rutherford cross section decreases exponentially at large angles for the heavy elements, and the differential cross sections break away from Rutherford behavior at angles which increase almost linearly with increase of atomic number of the target nucleus. A comparison of the results for natural tin, and tin enriched to 85% in Sn^{120}, indicated that within the experimental uncertainties over the measured angular interval, there were no pronounced isotopic effects. The data are presented both in tabular and graphical form to allow detailed comparison with theory.

ELASTIC SCATTERING OF 31-Mev He^3 IONS FROM SEVERAL ELEMENTS *

George Igo and Jose G. Vidal

Lawrence Radiation Laboratory
University of California
Berkeley, California

and

Samuel S. Markowitz

Chemistry Department and Lawrence Radiation Laboratory,
University of California, Berkeley, California

I. INTRODUCTION

Following the discovery of He^3 in 1939,[1] Barkas called attention to the advantages of using He^3 as a projectile for production and study of neutron-deficient nuclides.[2] The scarcity of He^3, however, precluded its extensive use. The natural abundance is only 1.3×10^{-4} atom percent of normal helium. Since the early 1950's, considerable He^3 has been produced by the beta-decay of tritium, in turn produced by the $Li^6(n,\alpha)H^3$ reaction in high-flux reactors. The use of He^3 as an incident particle has been discussed more recently,[3,4] and an extensive review article has been prepared by Bromley and Almqvist covering most of the He^3 reaction studies prior to June 1959.[5] However, this review omitted discussion of inelastic and elastic scattering of He^3 from nuclei.

Elastic scattering of protons and neutrons has been studied,[6] and the data compared with optical-model calculations;[7-10] deuteron studies [11-16] and data analyses[17-19] have been performed. Elastic scattering cross sections[20-28] and reaction excitation functions[29-40] have been measured for alpha particles of incident energy up to about 50 Mev. Analyses[17,21,28,41-46] of the alpha-particle measurements have dealt mainly with elastic scattering data; optical-model calculations, however, also predict the total-reaction cross sections,

and a comparison of theory with experiment has been made for alpha-induced reactions.[47,48] Elastic scattering studies have also been carried out with heavy ions such as carbon, nitrogen, oxygen, and neon.[49-56]

Experimental studies of elastic scattering of He^3 ions at moderate energies have been performed at Birmingham,[57-62] Los Alamos,[63] and Berkeley[64] and optical-model analyses have been made on some of the angular distributions.[65] The importance of He^3 as a probe of the nucleus has been amplified by the calculations of Hodgson.[66]

The purpose of the present research is to measure the elastic scattering of moderate-energy He^3 ions from various nuclides, so that subsequent analyses of the experimental results with the optical model can be made. It is also of interest to test whether there are differences in He^3 vs He^4 scattering owing to the spin 1/2 of the He^3 nucleus. The low binding energy of He^3 (7.7 Mev as compared to 28.2 Mev for He^4) should make it a sensitive probe of the nuclear surface.

II. EXPERIMENTAL PROCEDURE

A. Targets

The targets used were thin self-supporting foils of beryllium, aluminum, copper, tin of natural isotopic composition, tin enriched to 85% in Sn^{120}, and bismuth. They were chosen to span the parameter $A^{1/3}$, where A is the mass number. An important criterion was that the first excited states of the isotopes of the above elements have sufficient energy separation from the ground state to enable elastic scattering to be separated from inelastic. All targets were subjected to spectroscopic analysis, which showed that metal impurities were present at most in trace quantities in all the targets except beryllium,

for which upper limits of 0.5% of cadmium, thorium, and uranium were determined. The effects of metalic impurities in the targets on the data should be negligible. Oxygen, chemically combined or adsorbed on the surfaces of the copper, tin, or bismuth targets, should be small and without effect on the data because kinematic arguments indicate that He^3 ions scattered elastically from oxygen would be resolved from those scattered from the heavy nuclei. Thin aluminum foils are known to have a surface layer of oxygen present. A new procedure for activation-analysis using He^3 as the incident particle has shown that the amount of oxygen in 0.001-in. aluminum is approximately 0.03 atom percent;[67] this should not affect the scattering results. By the He^3 activation analysis, the amount of oxygen in the beryllium was found to be approx 3%; the detector resolution should minimize the effects of the oxygen impurity in the beryllium. The foils of copper, tin, and bismuth were made by evaporation; the aluminum and beryllium foils were commercially available. The foil thicknesses (in mg/cm^2) were: Be (5.13), Al (1.14 and 1.64), Cu (4.52), $Sn^{(nat)}$ (4.04), Sn^{120} (1.81), and Bi (5.24). Thicknesses were determined by weighing a known area with a microbalance; in addition, successively smaller areas were weighed to check for target uniformity.

B. Irradiations

The angular distribution measurements were carried out at the Berkeley heavy-ion linear accelerator[68] with a gas supply of 4% He^3 in He^4. The gas contained about 10^{-6}% tritium and 0.03% H_2. Knowledge of these impurities is important because the desired accelerated species was $He^3(+1)$, and $He^3(+1)$ and $H_3(+1)$ would be accelerated under the same conditions because of the same charge-to-mass ratio. While this would not contribute to elastically scattered He^3 events, false readings of the absolute He^3 beam current would be

obtained if any specie other than He^3 impinged on the Faraday cup. The low abundance of T_2 and H_2 in the gas supply indicated that even a preferential ionization of hydrogen over helium in the ion source of a factor of 10 would not interfere with the results. Tests have shown that He^4 ions will not be accelerated when the conditions are set for $He^3(+1)$. The energy of the beam was 31.2 Mev (10.4 Mev per nucleon).[68,69] The collimating system and bending magnet (see Fig. 1) restricted the energy spread to approx 2%. The beam pulses were checked to be 2 msec in length and the repetition rate was either 10 or 15 pulses per sec. The 2 or 3% duty cycle limited the rate at which the experimental data could be measured. The absolute beam intensity and total charge passing through the target were determined with a calibrated Faraday cup and integrating electrometer. In addition the relative intensity was monitored with a NaI(Tℓ) scintillation counter that detected elastically scattered He^3 ions at a fixed angle and geometry. The electrometer was calibrated by passing a known current through it for a measured time; the current source was a thermally insulated 1.019-volt standard cell using three precision resistors of 1.00×10^7, 1.00×10^8, and 1.00×10^9 ohms resistance. The average beam intensities were 0.1 to 100 mμa, depending on whether small or large angles were being measured. The Faraday cup was protected from low-energy electrons either by magnets or an electric potential.

The scattering chamber (Fig. 1) was evacuated and the system was open to the linear accelerator pumping system that gave a pressure of 10^{-5} mm Hg. The $He^3(+1)$ beam after magnetic deflection was constrained to a 0.125-in. diam circular spot on the target foil at the center of the chamber. The beam was stripped to $He^3(+2)$ in the first few μg of target material and then struck the Faraday cup. The various tantalum collimators used to define the beam are indicated in Fig. 1.

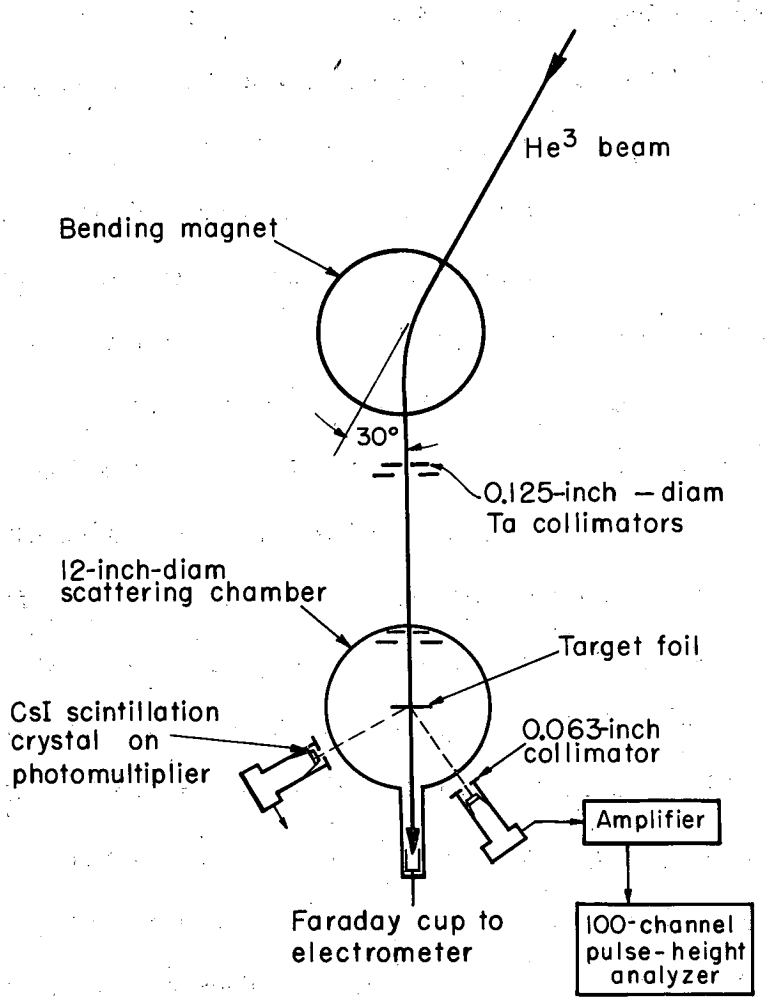

Fig. 1. Schematic diagram of scattering chamber and counters.

C. He^3 Detection

Those $He^3(+2)$ ions that were scattered passed through the 0.002-in. Mylar window of the chamber, approx 1 in. of air, and into the collimated CsI scintillation crystal detector. The CsI thickness was slightly greater than the range of a 31-Mev He^3 ion. The CsI was coupled to a photomultiplier tube. Pulse-height analysis was accomplished with a 100-channel analyzer after amplification of the output pulses from the photomultiplier. Two separate scintillation detectors were mounted on movable arms at a measured fixed radius from the center of the target foil. The angle with respect to the beam could be set within 0.2 deg by means of the marked dial which was also the chamber top. The detector collimators, tantalum rings, had apertures of either 0.0625- or 0.125-in. diam. For a 0.0625-in. collimator aperture, 6.46 in from the target the solid angle is 7.35×10^{-5} sr. The angular resolution was ~ 1 deg. Pulse-height resolution was ~ 3%. A pulse-height distribution is shown in Fig. 2.

The separation of elastic from inelastic events was considerably improved by placing a 70 mg/cm^2 aluminum absorber directly over the CsI crystals. The following example with copper illustrates the point: The range of a 31.0-Mev He^3 ion in aluminum is 133.5 mg/cm^2.[70] Because the first excited state in Cu^{65} is at 0.77 Mev, an inelastically scattered He^3 would have an energy of approx 30.2 Mev; the range in aluminum of the inelastic He^3 ions is 127.5 mg/cm^2. If, however, the ions pass through a 70 mg/cm^2 Al absorber, the residual ranges of the elastic He^3 ions and the inelastic He^3 ions will be 63.5 and 57.5 mg/cm^2, respectively, corresponding to energies of 20.2 and 19.0 Mev. A difference, therefore, of only 0.77 Mev in 31.0 or 2.6% will become a difference of 1.2 Mev in 20.2 or 5.9%, if advantage is taken of the greater rate of loss of energy for the inelastically scattered ions. Separation of elastic from inelastic events by pulse-height analysis is thus enhanced because

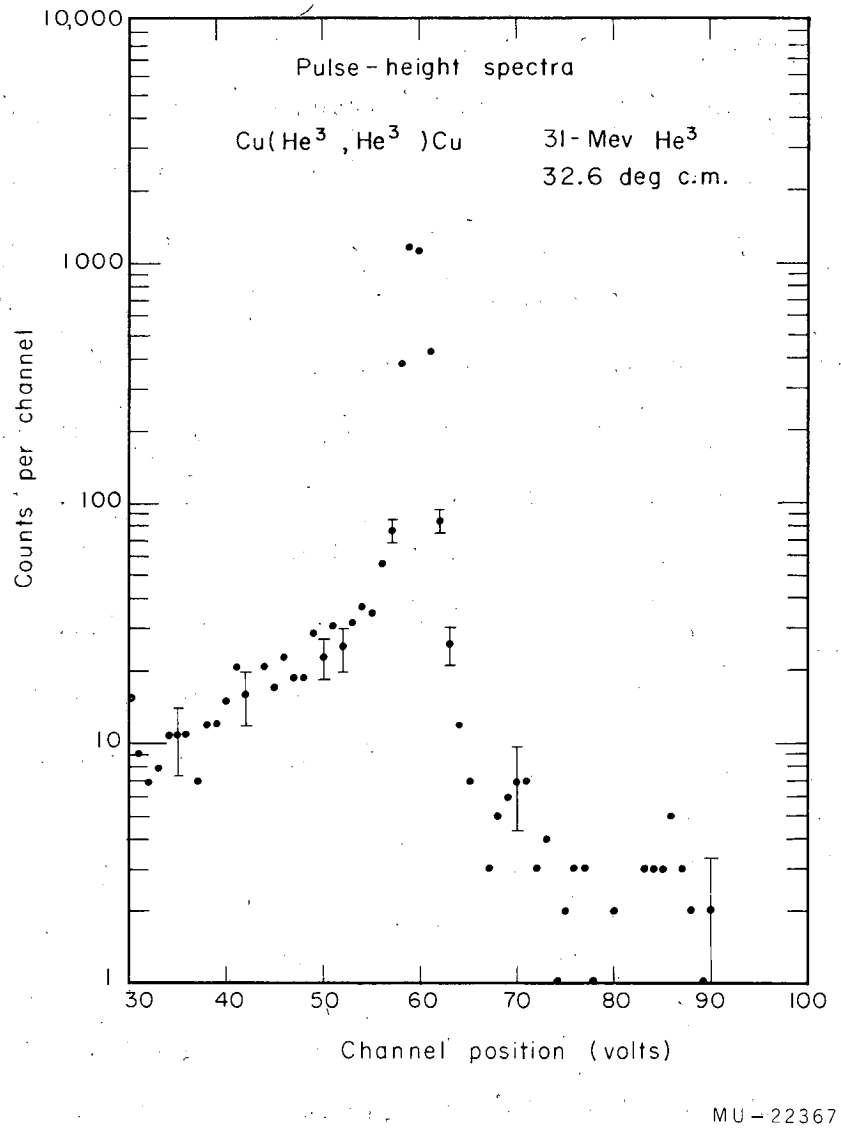

Fig. 2. Pulse-height spectrum for scattering from copper at 32.6 deg.

the energy spread of the incident beam is less than the energy resolution of the detectors.

The background in the region of the elastic scattering peak, in the pulse-height spectra obtained from the CsI counters, consisted of: (a) pulses due to α particles produced by the exoergic (He^3,α) reactions, (b) inelastically scattered He^3 ions, and (c) scattering from the tantalum collimators. The spectra were graphed on semilog paper, and the background was subtracted in a consistent manner with the aid of parabolic templates which were fitted to the elastic peak over regions where the background contribution was small. The magnitude of the background contribution varied with target and angle of observation as follows: For Bi between 10 and 98 deg, background varied from 0.7 to 1.6% of the peak area; for Sn^{120} between 20 and 120 deg, background was 0.5 to 13%; for Cu between 10 and 64 deg, background was 1 to 5%; for Al between 14 and 68 deg, background was 0.9 to 19%; and for Be between 17 and 65 deg, the background was 0.8 to 30%.

III. RESULTS AND DISCUSSION

The data are presented in Table I through VI, and in Figs. 3 through 9, to allow detailed comparison with any calculations. The Tables list the absolute differential cross section for elastic scattering of 31.2-Mev He^3 ions and the ratio of that cross section to the Rutherford cross section in the c.m. system as a function of angle. The general behavior is shown in the graphs, and in Fig. 9 the ratios are plotted for all the elements studied. The number of counts accumulated at most angles gave a standard deviation of approx 1.5%. The reproducibility of a series of points taken at the same angle which includes the effects of statistics, Faraday cup integrator readings, and graphical analysis was approx 2.3%. The individual datum was corrected for "dead-time"

Table I. The differential cross section for elastic scattering of 31.2-Mev He^3 ions incident on beryllium and the ratio of the experimental cross section to the Rutherford cross section in the center-of-mass system.

$\theta_{c.m.}$ (deg)	$(d\sigma/d\Omega)$ (barns/sr)	$\frac{(d\sigma/d\Omega)}{(d\sigma/d\Omega)_R}$
17.1	5.85×10^{-1}	1.86×10^{0}
19.7	2.01×10^{-1}	1.14×10^{0}
22.4	6.38×10^{-2}	4.09×10^{-1}
25.0	7.04×10^{-3}	1.02×10^{-1}
27.1	5.49×10^{-3}	1.09×10^{-1}
27.6	8.88×10^{-3}	1.89×10^{-1}
28.9	1.49×10^{-2}	3.82×10^{-1}
31.6	3.00×10^{-2}	1.09×10^{0}
32.9	2.92×10^{-2}	1.24×10^{0}
35.5	2.81×10^{-2}	1.60×10^{0}
36.8	2.57×10^{-2}	1.68×10^{0}
38.1	2.43×10^{-2}	1.81×10^{0}
38.6	2.36×10^{-2}	1.86×10^{0}
39.1	2.02×10^{-2}	1.66×10^{0}
39.4	1.95×10^{-2}	1.66×10^{0}
39.9	1.93×10^{-2}	1.72×10^{0}
42.5	1.03×10^{-2}	1.18×10^{0}
43.0	6.84×10^{-3}	8.13×10^{-1}
43.8	6.72×10^{-3}	8.57×10^{-1}
44.0	5.40×10^{-3}	7.02×10^{-1}
46.2	2.74×10^{-3}	4.28×10^{-1}
46.8	2.12×10^{-3}	3.47×10^{-1}
47.6	1.82×10^{-3}	3.19×10^{-1}
47.9	1.31×10^{-3}	2.35×10^{-1}
49.4	1.07×10^{-3}	2.15×10^{-1}
50.1	1.36×10^{-3}	2.88×10^{-1}
50.4	1.01×10^{-3}	2.18×10^{-1}
51.4	1.67×10^{-3}	3.89×10^{-1}
56.9	2.20×10^{-3}	7.51×10^{-1}
57.9	2.46×10^{-3}	8.95×10^{-1}
59.7	2.59×10^{-3}	1.05×10^{0}
60.7	2.48×10^{-3}	1.06×10^{0}
61.7	3.21×10^{-3}	1.46×10^{0}
64.6	1.82×10^{-3}	9.59×10^{-1}

Table II. The differential cross section for elastic scattering of 31.2-Mev He^3 ions incident on aluminum and the ratio of the experimental cross section to the Rutherford cross section in the center-of-mass system.

$\theta_{c.m.}$ (deg)	$(d\sigma/d\Omega)$ (barns/sr)	$\frac{(d\sigma/d\Omega)}{(d\sigma/d\Omega)_R}$
13.8	3.96×10^{0}	7.43×10^{-1}
14.9	2.45×10^{0}	6.22×10^{-1}
16.0	1.51×10^{0}	5.10×10^{-1}
18.2	5.32×10^{-1}	2.99×10^{-1}
19.3	3.51×10^{-1}	2.49×10^{-1}
20.4	2.54×10^{-1}	2.25×10^{-1}
20.6	2.37×10^{-1}	2.19×10^{-1}
21.5	2.36×10^{-1}	2.57×10^{-1}
21.7	2.29×10^{-1}	2.60×10^{-1}
22.9	2.34×10^{-1}	3.27×10^{-1}
23.9	2.39×10^{-1}	3.84×10^{-1}
24.0	2.17×10^{-1}	4.00×10^{-1}
26.2	2.03×10^{-1}	4.82×10^{-1}
27.2	1.58×10^{-1}	4.39×10^{-1}
28.3	1.26×10^{-1}	4.04×10^{-1}
29.5	9.60×10^{-2}	3.36×10^{-1}
30.6	6.97×10^{-2}	3.04×10^{-1}
31.7	4.00×10^{-2}	1.99×10^{-1}
32.3	3.53×10^{-2}	1.90×10^{-1}
32.6	2.67×10^{-2}	1.49×10^{-1}
32.8	2.59×10^{-2}	1.47×10^{-1}
34.8	8.70×10^{-3}	6.26×10^{-2}
34.9	8.92×10^{-3}	6.46×10^{-2}
35.8	7.77×10^{-3}	6.27×10^{-2}
37.0	7.71×10^{-3}	6.98×10^{-2}
37.2	9.90×10^{-3}	9.25×10^{-2}
38.2	1.36×10^{-2}	1.40×10^{-1}
39.1	1.20×10^{-2}	1.36×10^{-1}
40.2	1.43×10^{-2}	1.79×10^{-1}
40.4	1.63×10^{-2}	2.08×10^{-1}
42.4	1.51×10^{-2}	2.32×10^{-1}
43.5	1.36×10^{-2}	2.31×10^{-1}
43.7	1.37×10^{-2}	2.36×10^{-1}
44.6	1.18×10^{-2}	2.21×10^{-1}
45.9	9.33×10^{-3}	1.94×10^{-1}
46.9	7.89×10^{-3}	1.78×10^{-1}
48.0	5.24×10^{-3}	1.29×10^{-1}
48.9	3.67×10^{-3}	9.68×10^{-2}
51.2	1.19×10^{-3}	3.74×10^{-2}
52.2	1.02×10^{-3}	3.42×10^{-2}
53.4	9.68×10^{-4}	3.54×10^{-2}
54.5	1.29×10^{-3}	5.10×10^{-2}
55.4	1.29×10^{-3}	5.42×10^{-2}
57.7	2.12×10^{-3}	1.03×10^{-1}
58.6	1.80×10^{-3}	9.29×10^{-2}
60.9	1.93×10^{-3}	1.14×10^{-1}
61.8	1.41×10^{-3}	8.81×10^{-2}
64.0	1.05×10^{-3}	7.52×10^{-2}
65.0	8.18×10^{-4}	6.20×10^{-2}
67.2	3.94×10^{-4}	3.36×10^{-2}
68.1	3.73×10^{-4}	3.33×10^{-2}

Table III. The differential cross section for elastic scattering of 31.2-Mev He^3 ions incident on copper and the ratio of the experimental cross section to the Rutherford cross section in the center-of-mass system.

$\theta_{c.m.}$ (deg)	$(d\sigma/d\Omega)$ (barns/sr)	$\frac{(d\sigma/d\Omega)}{(d\sigma/d\Omega)_R}$
10.9	5.22×10^{1}	0.863×10^{0}
11.6	4.86×10^{1}	1.02×10^{0}
11.9	3.90×10^{1}	0.915×10^{0}
12.0	4.30×10^{1}	1.05×10^{0}
13.0	2.87×10^{1}	0.959×10^{0}
14.0	1.93×10^{1}	0.864×10^{0}
14.1	2.02×10^{1}	0.933×10^{0}
15.1	1.24×10^{1}	0.748×10^{0}
16.1	8.65×10^{0}	0.676×10^{0}
16.2	1.06×10^{1}	0.846×10^{0}
17.1	6.26×10^{0}	0.620×10^{0}
18.2	4.50×10^{0}	0.572×10^{0}
18.3	4.84×10^{0}	0.630×10^{0}
19.2	3.33×10^{0}	0.524×10^{0}
20.4	2.59×10^{0}	0.519×10^{0}
21.7	1.59×10^{0}	0.408×10^{0}
22.3	1.54×10^{0}	0.438×10^{0}
23.2	1.17×10^{0}	0.387×10^{0}
23.8	1.00×10^{0}	0.369×10^{0}
25.9	6.18×10^{-1}	0.325×10^{0}
26.7	5.01×10^{-1}	0.294×10^{0}
27.9	3.57×10^{-1}	0.251×10^{0}
30.0	2.16×10^{-1}	0.198×10^{0}
30.3	1.71×10^{-1}	0.163×10^{0}
30.7	1.83×10^{-1}	0.184×10^{0}
32.1	1.40×10^{-1}	0.167×10^{0}
32.6	1.38×10^{-1}	0.174×10^{0}
34.2	1.11×10^{-1}	0.172×10^{0}
34.7	1.04×10^{-1}	0.169×10^{0}
35.0	1.20×10^{-1}	0.199×10^{0}
38.3	5.68×10^{-2}	0.134×10^{0}
38.9	4.99×10^{-2}	0.125×10^{0}
42.5	2.23×10^{-2}	0.784×10^{-1}
43.0	1.99×10^{-2}	0.733×10^{-1}
46.6	1.33×10^{-2}	0.665×10^{-1}
47.6	1.37×10^{-2}	0.741×10^{-1}
50.8	8.76×10^{-3}	0.604×10^{-1}
51.9	7.91×10^{-3}	0.590×10^{-1}
54.9	3.95×10^{-3}	0.365×10^{-1}
55.4	3.41×10^{-3}	0.325×10^{-1}
59.0	2.11×10^{-3}	0.253×10^{-1}
59.5	2.04×10^{-3}	0.252×10^{-1}
63.1	1.88×10^{-3}	0.288×10^{-1}
63.6	1.74×10^{-3}	0.273×10^{-1}

Table IV. The differential cross section for elastic scattering of 31.2-Mev He^3 ions incident on tin of natural isotopic composition and the ratio of the experimental cross section to the Rutherford cross section in the c. m. system.

$\theta_{c.m.}$ (deg)	$(d\sigma/d\Omega)$ (barns/sr)	$\frac{(d\sigma/d\Omega)}{(d\sigma/d\Omega)_R}$
10.7	1.82×10^{2}	1.00×10^{0}
11.7	1.33×10^{2}	1.04×10^{0}
12.7	9.30×10^{1}	9.94×10^{-1}
13.7	7.13×10^{1}	1.03×10^{0}
14.7	5.58×10^{1}	1.07×10^{0}
15.8	4.32×10^{1}	1.10×10^{0}
16.8	3.31×10^{1}	1.08×10^{0}
17.8	2.80×10^{1}	1.15×10^{0}
18.9	2.25×10^{1}	1.17×10^{0}
19.2	2.20×10^{1}	1.22×10^{0}
20.2	1.62×10^{1}	1.09×10^{0}
21.2	1.30×10^{1}	1.06×10^{0}
22.2	1.06×10^{1}	1.04×10^{0}
23.3	9.04×10^{0}	1.07×10^{0}
24.3	7.12×10^{0}	9.99×10^{-1}
26.2	4.15×10^{0}	7.83×10^{-1}
26.3	4.70×10^{0}	9.01×10^{-1}
28.4	2.80×10^{0}	7.30×10^{-1}
29.7	2.29×10^{0}	7.07×10^{-1}
30.1	2.00×10^{0}	6.50×10^{-1}
30.4	1.88×10^{0}	6.35×10^{-1}
31.0	1.79×10^{0}	6.54×10^{-1}
32.1	1.49×10^{0}	6.22×10^{-1}
32.4	1.33×10^{0}	5.75×10^{-1}
33.1	1.13×10^{0}	5.32×10^{-1}
34.5	8.67×10^{-1}	4.79×10^{-1}
35.1	7.84×10^{-1}	4.64×10^{-1}
37.2	5.48×10^{-1}	4.03×10^{-1}
37.6	5.40×10^{-1}	4.15×10^{-1}
39.2	4.01×10^{-1}	3.62×10^{-1}
41.2	2.74×10^{-1}	3.00×10^{-1}
43.7	1.89×10^{-1}	2.60×10^{-1}
46.3	1.33×10^{-1}	2.27×10^{-1}
46.7	1.21×10^{-1}	2.18×10^{-1}
47.4	1.04×10^{-1}	1.94×10^{-1}
49.4	7.39×10^{-2}	1.61×10^{-1}
52.8	5.01×10^{-2}	1.40×10^{-1}
53.4	4.24×10^{-2}	1.23×10^{-1}
54.9	3.79×10^{-2}	1.22×10^{-1}
56.9	3.05×10^{-2}	1.12×10^{-1}
57.5	2.68×10^{-2}	1.03×10^{-1}
60.9	1.98×10^{-2}	9.33×10^{-2}
61.6	1.77×10^{-2}	8.68×10^{-2}

Table V. The differential cross section for elastic scattering of 31.2-Mev He^3 ions incident on tin enriched to 85% in Sn^{120} and the ratio of the experimental cross section to the Rutherford cross section in the c. m. system.

$\theta_{c.m.}$ (deg)	$(d\sigma/d\Omega)$ (barns/sr)	$\frac{(d\sigma/d\Omega)}{(d\sigma/d\Omega)_R}$
20.8	9.85×10^{0}	7.46×10^{-1}
25.9	3.48×10^{0}	6.33×10^{-1}
31.0	1.28×10^{0}	4.67×10^{-1}
36.1	5.67×10^{-1}	3.75×10^{-1}
41.2	2.39×10^{-1}	6.62×10^{-1}
46.3	1.19×10^{-1}	2.03×10^{-1}
51.4	5.80×10^{-2}	1.46×10^{-1}
56.5	2.93×10^{-2}	8.71×10^{-2}
60.9	1.80×10^{-2}	8.49×10^{-2}
61.6	1.73×10^{-2}	8.48×10^{-2}
66.6	7.90×10^{-3}	5.13×10^{-2}
69.0	5.90×10^{-3}	4.32×10^{-2}
71.7	4.84×10^{-3}	4.07×10^{-2}
75.1	3.33×10^{-3}	3.30×10^{-2}
77.7	2.50×10^{-3}	2.77×10^{-2}
81.1	1.76×10^{-3}	2.24×10^{-2}
83.7	1.23×10^{-3}	1.74×10^{-2}
86.1	1.11×10^{-3}	1.72×10^{-2}
92.1	6.31×10^{-4}	1.21×10^{-2}
95.7	4.25×10^{-4}	9.18×10^{-3}
98.1	3.84×10^{-4}	8.93×10^{-3}
101.7	2.48×10^{-4}	6.41×10^{-3}
104.1	2.04×10^{-4}	5.64×10^{-3}
107.7	1.45×10^{-4}	4.39×10^{-3}
112.0	1.07×10^{-4}	3.61×10^{-3}
113.6	1.03×10^{-4}	3.61×10^{-3}
116.0	1.01×10^{-4}	3.74×10^{-3}
119.6	7.06×10^{-5}	2.81×10^{-3}

Table VI. The differential cross section for elastic scattering of 31.2-Mev He^3 ions incident on bismuth and the ratio of the experimental cross section to the Rutherford cross section in the center-of-mass system.

$\theta_{c.m.}$ (deg)	$(d\sigma/d\Omega)$ (barns/sr)	$\frac{(d\sigma/d\Omega)}{(d\sigma/d\Omega)_R}$
10.6	4.86×10^{2}	9.36×10^{-1}
11.2	3.66×10^{2}	8.78×10^{-1}
11.6	3.59×10^{2}	9.89×10^{-1}
12.6	2.39×10^{2}	9.16×10^{-1}
13.6	1.79×10^{2}	9.32×10^{-1}
14.6	1.31×10^{2}	9.04×10^{-1}
15.6	9.91×10^{1}	8.93×10^{-1}
16.6	8.09×10^{1}	9.30×10^{-1}
17.7	6.26×10^{1}	9.43×10^{-1}
18.7	5.16×10^{1}	9.43×10^{-1}
18.9	4.68×10^{1}	9.00×10^{-1}
19.9	3.91×10^{1}	9.24×10^{-1}
20.9	3.13×10^{1}	8.97×10^{-1}
21.2	2.96×10^{1}	8.97×10^{-1}
21.5	2.71×10^{1}	8.69×10^{-1}
22.1	2.41×10^{1}	8.61×10^{-1}
22.9	2.05×10^{1}	8.44×10^{-1}
23.0	2.14×10^{1}	8.95×10^{-1}
23.1	2.00×10^{1}	8.51×10^{-1}
24.1	1.63×10^{1}	8.19×10^{-1}
25.0	1.40×10^{1}	8.14×10^{-1}
25.1	1.47×10^{1}	8.70×10^{-1}
26.0	1.19×10^{1}	8.10×10^{-1}
26.1	1.13×10^{1}	7.79×10^{-1}
27.0	1.11×10^{1}	8.74×10^{-1}
27.2	1.02×10^{1}	8.23×10^{-1}
29.0	9.02×10^{0}	9.40×10^{-1}
29.2	8.74×10^{0}	9.35×10^{-1}
29.8	7.67×10^{0}	8.87×10^{-1}
30.2	6.97×10^{0}	8.51×10^{-1}
30.7	6.49×10^{0}	8.44×10^{-1}
30.8	6.94×10^{0}	9.15×10^{-1}
31.0	6.78×10^{0}	9.17×10^{-1}
31.2	6.52×10^{0}	9.03×10^{-1}
31.7	6.50×10^{0}	9.59×10^{-1}
31.8	6.37×10^{0}	9.50×10^{-1}
32.2	5.83×10^{0}	9.14×10^{-1}
32.9	5.63×10^{0}	9.59×10^{-1}
33.2	5.22×10^{0}	9.17×10^{-1}
33.9	5.43×10^{0}	1.04×10^{0}
34.2	4.64×10^{0}	9.19×10^{-1}
34.7	4.27×10^{0}	8.93×10^{-1}
34.9	4.77×10^{0}	1.03×10^{0}
35.1	4.58×10^{0}	1.00×10^{0}
35.2	4.05×10^{0}	8.96×10^{-1}
35.7	3.97×10^{0}	9.30×10^{-1}
36.8	3.52×10^{0}	9.26×10^{-1}
36.9	3.75×10^{0}	9.97×10^{-1}
37.1	3.51×10^{0}	9.54×10^{-1}
37.8	3.32×10^{0}	9.68×10^{-1}
37.9	3.27×10^{0}	9.62×10^{-1}
38.8	2.94×10^{0}	9.51×10^{-1}

Table VI. Bi + 31.2-Mev He^3 (continued)

$\theta_{c.m.}$ (deg)	$(d\sigma/d\Omega)$ (barns/sr)	$\frac{(d\sigma/d\Omega)}{(d\sigma/d\Omega)_R}$
38.9	3.15×10^{0}	1.03×10^{0}
39.1	2.73×10^{0}	9.05×10^{-1}
39.8	2.50×10^{0}	8.87×10^{-1}
40.8	2.19×10^{0}	8.55×10^{-1}
40.9	2.37×10^{0}	9.37×10^{-1}
41.2	2.47×10^{0}	1.00×10^{0}
41.8	1.88×10^{0}	8.07×10^{-1}
43.0	1.94×10^{0}	9.28×10^{-1}
43.8	1.56×10^{0}	8.00×10^{-1}
45.0	1.49×10^{0}	8.47×10^{-1}
45.2	1.50×10^{0}	8.67×10^{-1}
47.0	1.29×10^{0}	8.66×10^{-1}
47.4	1.06×10^{0}	7.36×10^{-1}
47.9	9.63×10^{-1}	6.93×10^{-1}
49.2	9.46×10^{-1}	7.51×10^{-1}
51.3	8.24×10^{-1}	7.63×10^{-1}
51.4	6.97×10^{-1}	6.51×10^{-1}
51.9	6.33×10^{-1}	6.15×10^{-1}
52.1	6.31×10^{-1}	6.25×10^{-1}
54.3	5.43×10^{-1}	6.28×10^{-1}
55.3	5.78×10^{-1}	7.11×10^{-1}
55.5	4.47×10^{-1}	5.57×10^{-1}
55.9	4.00×10^{-1}	5.12×10^{-1}
56.1	4.70×10^{-1}	6.08×10^{-1}
58.1	3.61×10^{-1}	5.32×10^{-1}
59.3	3.01×10^{-1}	4.78×10^{-1}
59.5	2.78×10^{-1}	4.47×10^{-1}
60.1	3.29×10^{-1}	5.48×10^{-1}
61.5	2.19×10^{-1}	3.97×10^{-1}
62.0	1.92×10^{-1}	3.58×10^{-1}
63.3	2.29×10^{-1}	4.60×10^{-1}
64.2	2.01×10^{-1}	4.27×10^{-1}
65.5	1.68×10^{-1}	3.81×10^{-1}
66.0	1.40×10^{-1}	3.26×10^{-1}
66.4	1.55×10^{-1}	3.69×10^{-1}
67.4	1.57×10^{-1}	3.94×10^{-1}
68.2	1.33×10^{-1}	3.47×10^{-1}
70.2	9.35×10^{-2}	2.71×10^{-1}
72.2	9.91×10^{-2}	3.16×10^{-1}
75.4	7.67×10^{-2}	2.84×10^{-1}
76.2	6.32×10^{-2}	2.42×10^{-1}
79.4	5.31×10^{-2}	2.34×10^{-1}
80.2	4.79×10^{-2}	2.19×10^{-1}
81.5	3.72×10^{-2}	1.79×10^{-1}
83.4	3.70×10^{-2}	1.92×10^{-1}
84.2	3.38×10^{-2}	1.82×10^{-1}
88.2	2.31×10^{-2}	1.43×10^{-1}
90.4	2.03×10^{-2}	1.36×10^{-1}
92.2	1.55×10^{-2}	1.11×10^{-1}
94.4	1.45×10^{-2}	1.12×10^{-1}
98.4	9.69×10^{-3}	8.43×10^{-2}

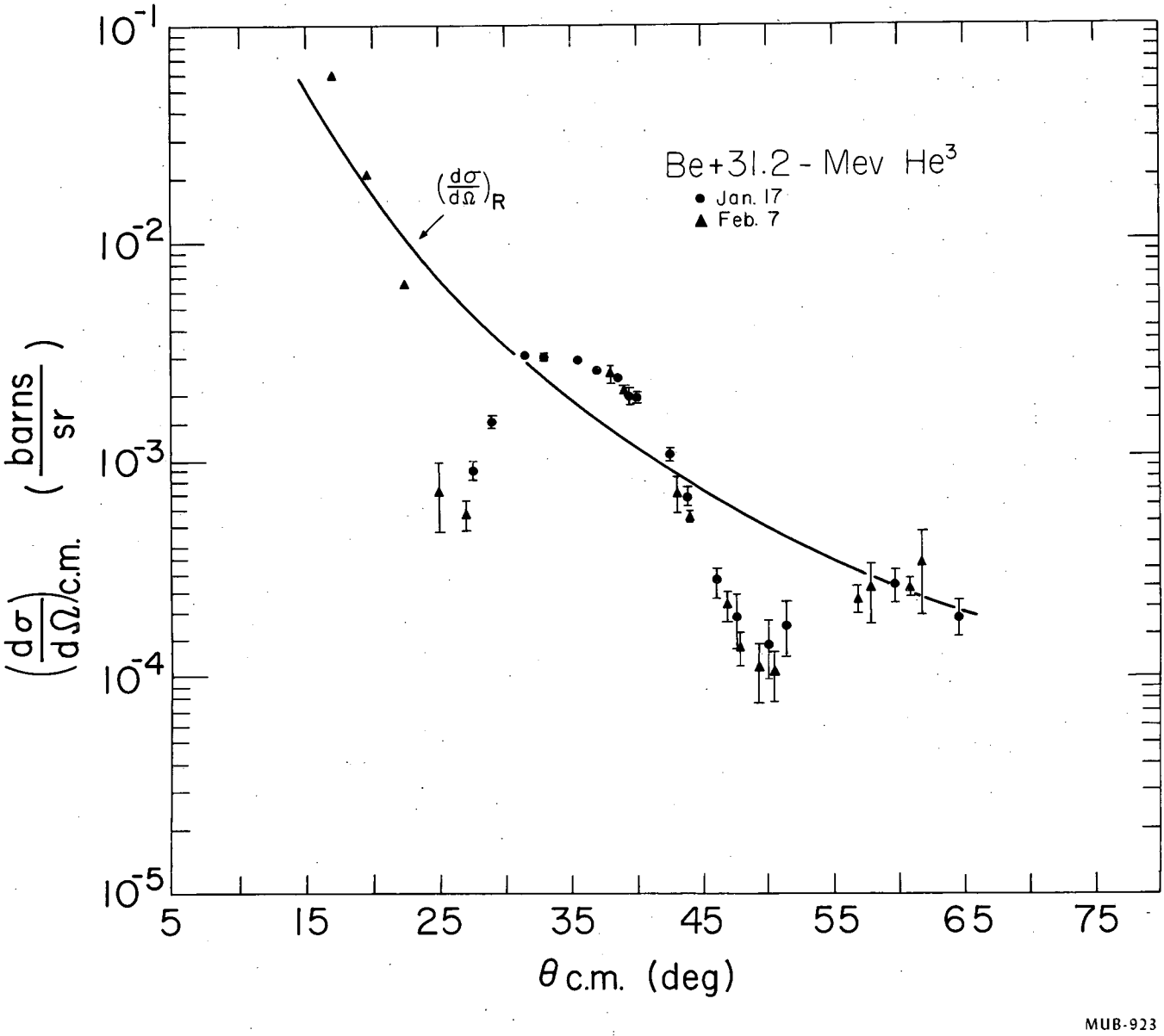

Fig. 3. Angular distribution for elastic scattering of 31.2-Mev He^3 ions from beryllium. The symbols indicate the experimental points and their standard deviations; the solid line is the calculated differential cross section for Rutherford scattering in the center-of-mass system.

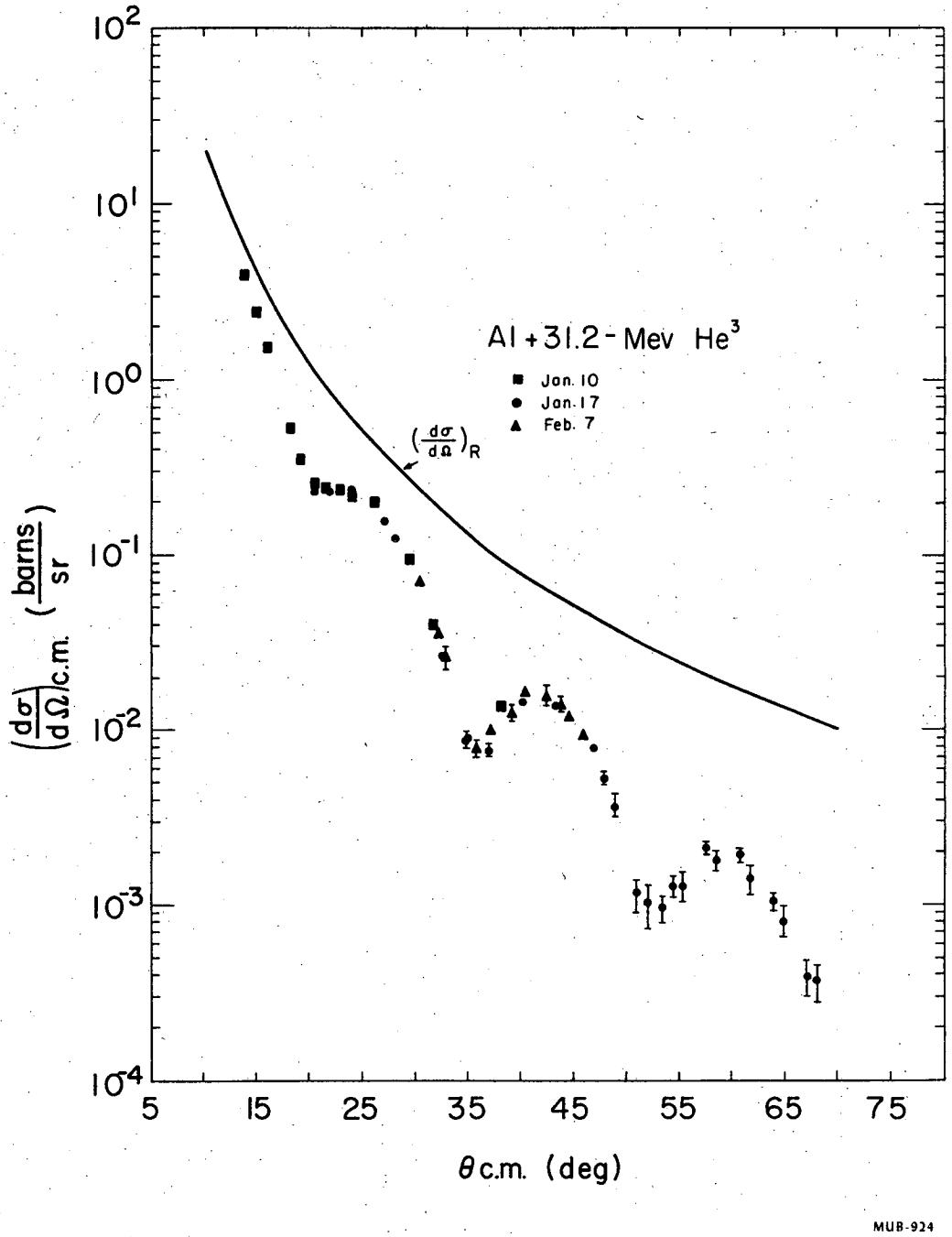

Fig. 4. Angular distribution for elastic scattering of 31.2-Mev He^3 ions from aluminum. The symbols indicate the experimental points and their standard deviations; the solid line is the calculated differential cross section for Rutherford scattering in the c.m. system.

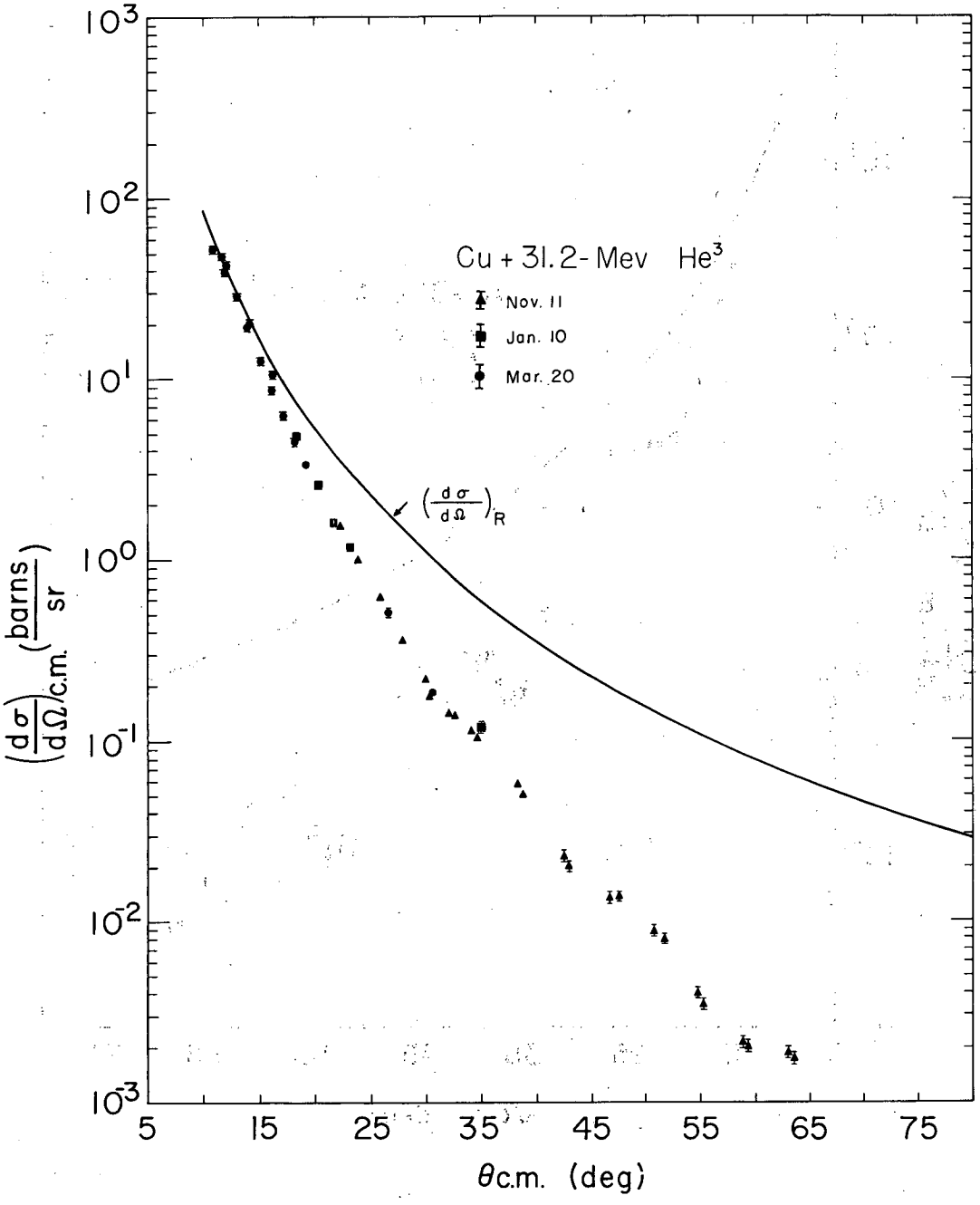

Fig. 5. Angular distribution for elastic scattering of 31.2-Mev He^3 ions from copper. The symbols indicate the experimental points and their standard deviations; the solid line is the calculated differential cross section for Rutherford scattering in the c.m. system.

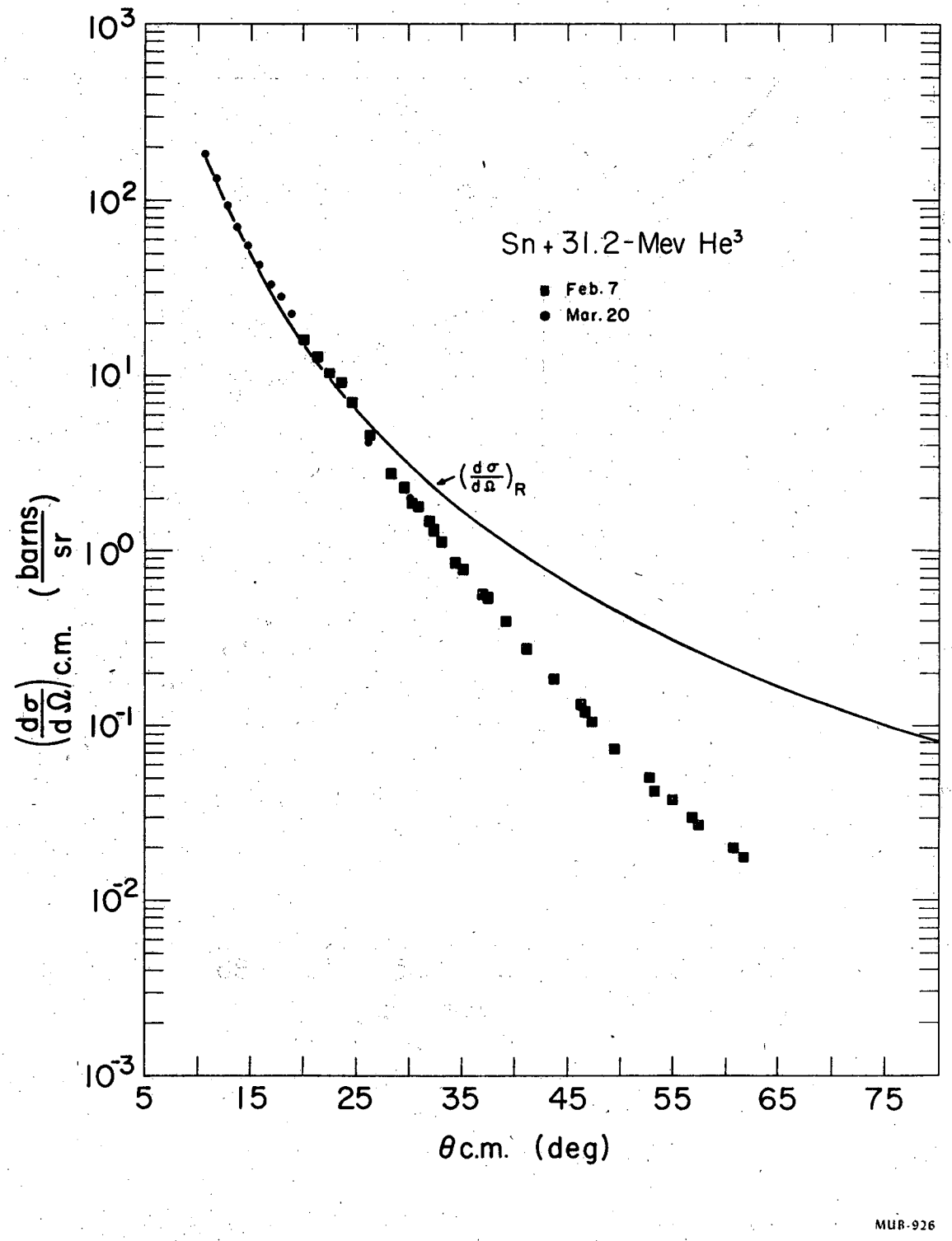

Fig. 6. Angular distribution for elastic scattering of 31.2-Mev He^3 ions from tin of natural isotopic composition. The symbols indicate the experimental points and their standard deviations; the solid line is the calculated differential cross section for Rutherford scattering in the c.m. system.

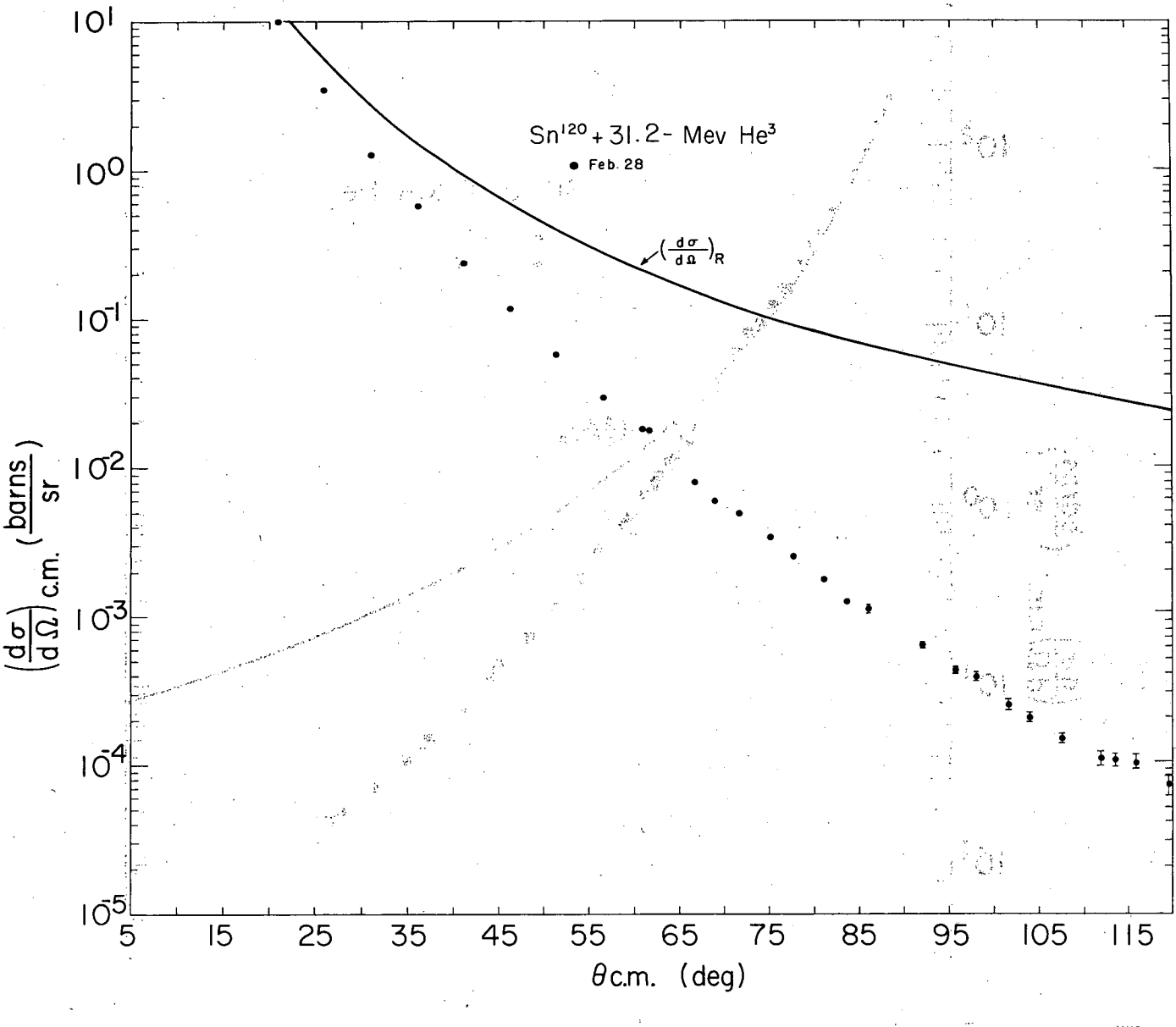

Fig. 7. Angular distribution for elastic scattering of 31.2-Mev He^3 ions from tin enriched to 85% in Sn^{120}. The symbols indicate the experimental points and their standard deviations; the solid line is the calculated differential cross section for Rutherford scattering in the c.m. system.

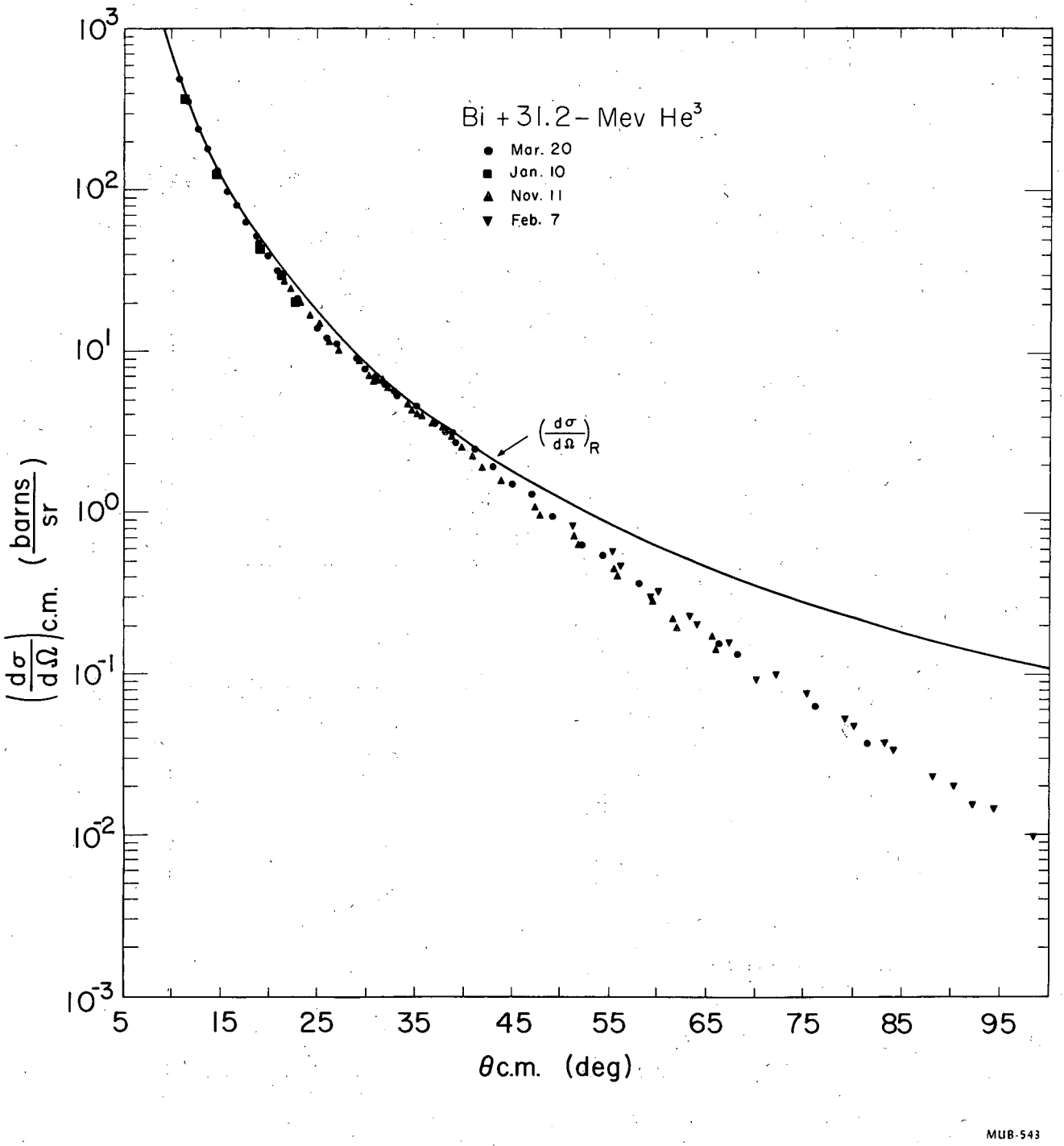

Fig. 8. Angular distribution for elastic scattering of 31.2-Mev He^3 ions from bismuth. The symbols indicate the experimental points and their standard deviations; the solid line is the calculated differential cross section for Rutherford scattering in the c.m. system.

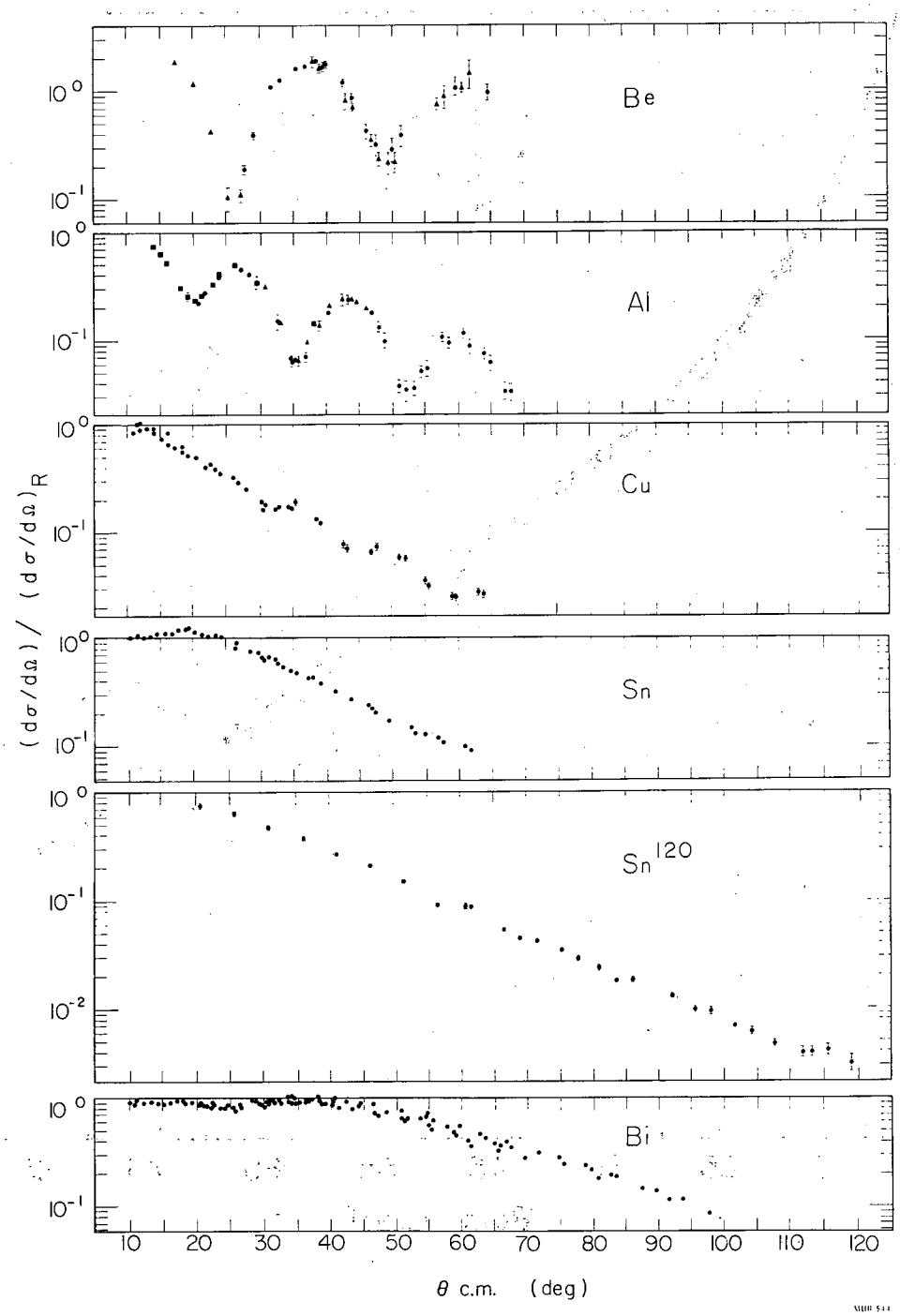

Fig. 9. The ratio of the experimental differential elastic scattering cross sections to the Rutherford scattering cross sections for 31.2-Mev He^3 ions incident on various elements. The scale of the ordinate is divided between the elements.

loss in the 100-channel analyzer; because the duty cycle of the accelerator was only 2 or 3%, the beam intensity was always limited so that the maximum average analyzer "dead-time" was 0.1%. This corresponded to a maximum "dead time" correction of either 5 or 3.3%, depending on the duty cycle. Errors in reading the "dead-time" would cause errors of approx 1% at most in the measured cross sections. The largest uncertainties are for beryllium and aluminum, where the background corrections are relatively large at large angles. The error flags in the figures are rms standard deviations of the uncertainties in the data.

The He^3 beam did not pass precisely through the zero degree dial setting of the scattering chamber, and therefore a correction was made to translate the "dial" angle into the true laboratory angle. This correction, determined by obtaining data with both of the detectors over a series of angles, amounted to 0.6 deg; the error in this correction is approx 0.2 deg. The error in the listed c.m. angles is therefore 0.2 deg.

The results for aluminum agree well with the data of Greenlees, Lilley, Rowe, and Hodgson[61] at 29.1 Mev, but the copper results differ. Our measurements for copper are lower by approx 40%. The tin results are in reasonable agreement with the data of Greenlees and Rowe at 29.1 Mev,[60] although the present results are systematically smaller by approx 25% beyond 40 deg. There are no data to compare with the beryllium and bismuth results. It is possible that the difference between the bombarding energies can account for the difference in the cross sections for copper and tin.

The light element angular distributions show strong diffraction effects. For the heavy elements, the differential cross sections break away from Rutherford behavior at angles that increase with increasing atomic number. The "break-away" angle varies almost linearly with atomic number, the angles being approx 13, 25, and 42 deg for Cu, Sn, and Bi, respectively. Beyond the break-

away angle, the ratios of the cross sections decrease exponentially. In copper some diffraction effects are still observed at large angles.

A comparison of the results for natural tin and Sn^{120} indicates that, within the experimental uncertainties over the measured angular interval, there are no pronounced isotopic effects.

Optical-model analyses for He^3 elastic scattering at 29 Mev [61,62] have indicated that the differential cross sections were more sensitive to the nuclear radius and the surface diffuseness than to the depth of the refracting and absorbing nuclear potentials. This suggests that elastic scattering is, at these energies, predominantly a surface interaction.

ACKNOWLEDGEMENTS

Communication of results to us by Professor W. E. Burcham prior to publication is deeply appreciated. It is a pleasure to acknowledge Messrs. D. G. O'Connell and G. E. Steers for preparation of uniform, self-supporting targets for this research. The spectroscopic analyses were performed by Mr. G. V. Shalimoff, whose help we gratefully acknowledge. The cooperation of the crew of the heavy-ion linear accelerator is gratefully acknowledged.

REFERENCES

* This research was performed under the auspices of the U. S. Atomic Energy Commission.

1. L. W. Alvarez and R. Cornog, Phys. Rev. 56, 613 (1939).
2. W. H. Barkas, Phys. Rev. 56, 1242 (1939).
3. S. S. Markowitz and J. M. Hall, Bull. Am. Phys. Soc., Ser. II, 4, 8 (1959) and University of California Radiation Laboratory Report UCRL-8618, Jan. 1959.
4. D. R. F. Cochran and J. D. Knight, Bull. Am. Phys. Soc., Ser. II, 3, 323 (1958).
5. D. A. Bromley and E. Almqvist, Rep. Progr. Phys. 23, 544 (1960) and Atomic Energy of Canada, Ltd., Report CRP-881, AECL-950, 1959.
6. N. M. Hintz, Phys. Rev. 106, 1201 (1957).
7. S. Fernbach, R. Serber, and T. B. Taylor, Phys. Rev. 75, 1352 (1949).
8. H. Feshbach, C. E. Porter, and V. F. Weiskopf, Phys. Rev. 96, 448 (1954).
9. H. Feshbach, Ann. Rev. Nuclear Sci. 8, 49 (1958).
10. Proceedings of the International Conference on the Nuclear Optical Model, Florida State University Studies, No. 32. (Florida State University, Tallahassee, Florida, 1959).
11. G. Igo, W. Lorenz, and U. Schmidt-Rohr, Phys. Rev. 124, 832 (1961).
12. I. Slaus and W. P. Alford, Phys. Rev. 114, 1054 (1959).
13. J. R. Rees and M. P. Sampson, Phys. Rev. 108, 1289 (1957).
14. W. Cindro and N. S. Wall, Phys. Rev. 119, 1340 (1960).
15. H. E. Gove, Phys. Rev. 99, 1353 (1955).
16. J. L. Yntema, Phys. Rev. 114, 820 (1959), ibid. 113, 261 (1959).
17. C. E. Porter, Phys. Rev. 99, 1400 (1955).
18. M. A. Melkanoff, reference 10, p. 207.
19. J. B. A. England, R. McKeague, and P. E. Hodgson, Nuclear Phys. 16, 52 (1960).
20. G. W. Farwell and H. E. Wegner, Phys. Rev. 95, 1212 (1954).

REFERENCES (Cont)

21. N. S. Wall, J. R. Rees, and K. W. Ford, Phys. Rev. 97, 726 (1955).
22. H. E. Wegner, R. Eisberg, and G. Igo, Phys. Rev. 99, 825 (1955).
23. R. Ellis and L. Schecter, Phys. Rev. 101, 636 (1956).
24. R. Eisberg, G. Igo, and H. E. Wegner, Phys. Rev. 99, 1606 (1955).
25. E. Bleuler and D. J. Tendam, Phys. Rev. 99, 1605 (1955).
26. G. Igo, H. E. Wegner, and R. Eisberg, Phys. Rev. 101, 1508 (1956).
27. L. Seidlitz, E. Bleuler, and D. J. Tendam, Phys. Rev. 110, 682 (1958).
28. D. D. Kerlee, J. S. Blair, and G. W. Farwell, Phys. Rev. 107, 1343 (1957).
29. R. L. Walker, Phys. Rev. 76, 244 (1949).
30. I. Halpern, Phys. Rev. 76, 248 (1949).
31. S. N. Ghoshal, Phys. Rev. 80, 939 (1950).
32. J. M. Miller, G. Friedlander, and S. S. Markowitz, Phys. Rev. 98, 1197 (1955).
33. F. S. Houck and J. M. Miller, Phys. Rev. 123, 231 (1961).
34. K. G. Porges, Phys. Rev. 101, 225 (1956).
35. E. Bleuler, A. K. Stebbins, and D. J. Tendam, Phys. Rev. 90, 460 (1953).
36. E. Kelly and E. Segrè, Phys. Rev. 75, 999 (1949).
37. N. T. Porile, Phys. Rev. 115, 939 (1959).
38. N. T. Porile and D. L. Morrison, 116, 1193 (1959).
39. R. Vandenbosch, T. D. Thomas, S. Vandenbosch, R. A. Glass, and G. T. Seaborg, Phys. Rev. 111, 1358 (1958).
40. R. A. Glass, R. J. Carr, J. W. Cobble, and G. T. Seaborg, Phys. Rev. 104, 434 (1956).
41. J. S. Blair, Phys. Rev. 95, 1218 (1954).
42. N. Oda and K. Harada, Progr. Theoret. Phys. (Kyoto) 15, 545 (1956).
43. C. B. O. Mohr and B. A. Robson, Proc. Phys. Soc. (London) A69, 365 (1956).
44. G. Igo and R. M. Thaler, Phys. Rev. 106, 126 (1957).

REFERENCES (Cont)

45. W. B. Cheston and A. E. Glassgold, Phys. Rev. 106, 1215 (1957).

46. G. Igo. Phys. Rev. Letters 1, 167 (1958).

47. G. Igo, Phys. Rev. 115, 1665 (1959).

48. R. M. Eisberg and C. E. Porter, Revs. Modern Phys. 33, 190 (1961).

49. H. L. Reynolds and A. Zucker, Phys. Rev. 102, 1378 (1956).

50. E. Goldberg and H. L. Reynolds, Phys. Rev. 112, 1981 (1959); and Bull. Am. Phys. Soc., Ser. II, 4, 253 (1959).

51. J. A. McIntyre, S. D. Baker, and T. L. Watts, Phys. Rev. 116, 1212 (1959).

52. M. L. Halbert and A. Zucker, Phys. Rev. 115, 1635 (1959).

53. M. L. Halbert, C. E. Hunting, and A. Zucker, Phys. Rev. 117, 1545 (1960).

54. C. E. Porter, Phys. Rev. 112, 1722 (1957).

55. J. Alster, Heavy-Ion Elastic Scattering (Ph.D. thesis), University of California Radiation Laboratory Report UCRL-9650, April 1961 (unpublished).

56. Proceedings of the Conference on Reactions between Complex Nuclei, Gatlinburg, Tennessee, Oak Ridge National Laboratory Report ORNL-2606, 1958 (unpublished).

57. J. S. C. McKee, D. R. Sweetman, P. V. March, W. T. Toner, and W. M. Gibson, Phys. Rev. 115, 143 (1959).

58. D. J. Bredin, J. B. A. England, D. Evans, J. S. C. McKee, P. V. March, E. M. Mosinger, and W. T. Toner, Proc. Roy. Soc. (London) A258, 202 (1960).

59. J. Aguilar, W. E. Burcham, J. B. A. England, A. Garcia, P. E. Hodgson, P. V. March, J. S. C. McKee, E. M. Mosinger, and W. T. Toner, Proc. Roy. Soc. (London) A257, 13 (1960).

60. G. W. Greenlees and P. C. Rowe, Nuclear Phys. 15, 687 (1960).

61. G. W. Greenlees, J. S. Lilley, P. C. Rowe, and P. E. Hodgson, Nuclear Phys. 24, 334 (1961).

REFERENCES (Cont)

62. J. Aguilar, A. Garcia, J. B. A. England, P. E. Hodgson, and W. T. Toner, Nuclear Phys. 25, 259 (1961).

63. H. E. Wegner and W. S. Hall, Bull. Am. Phys. Soc., Ser.II, 3, 338 (1958); and private communication from H. E. W.

64. G. Igo, J. G. Vidal, and S. S. Markowitz, Bull. Am. Phys. Soc., Ser.II, 5, 229 (1960).

65. P. E. Hodgson, Nuclear Phys. 21, 28 (1960).

66. P. E. Hodgson, Nuclear Phys. 23, 499 (1961).

67. S. S. Markowitz and J. D. Mahony, Anal. Chem. (in press) and University of California Radiation Laboratory Report UCRL-9908, Nov. 1961.

68. E. L. Hubbard, W. R. Baker, K. W. Ehlers, H. S. Gordon, R. M. Main, N. J. Norris, R. Peters, L. Smith, C. M. Van Atta, F. Voelker, C. E. Anderson, R. Beringer, R. L. Gluckstern, W. J. Knox, M. J. Malkin, A. R. Quinton, L. Schwarcz, and G. W. Wheeler, Rev. Sci. Instr. 32, 621 (1961).

69. H. H. Heckman, B. L. Perkins, W. G. Simon, F. M. Smith, and W. H. Barkas, Phys. Rev. 117, 544 (1960).

70. H. Bichsel, Phys. Rev. 112, 1089 (1958).